Quantum logic with cavity photons from single atoms

Annemarie Holleczek,[1] Oliver Barter,[1] Allison Rubenok,[2] Jerome Dilley,[1]
Peter B. R. Nisbet-Jones,[1,3] Gunnar Langfahl-Klabes,[1] Graham D. Marshall,[2] Chris Sparrow,[2,4]
Jeremy L. O'Brien,[2] Konstantinos Poulios,[2,5] Axel Kuhn,[1] and Jonathan C. F. Matthews[2]

[1] *University of Oxford, Clarendon Laboratory, Parks Road, Oxford OX1 3PU, UK*
[2] *Centre for Quantum Photonics, H. H. Wills Physics Laboratory and Department of Electrical and Electronic Engineering, University of Bristol, Bristol BS8 1UB, UK*
[3] *now at: National Physics Laboratory, Teddington TW11 OLW, UK*
[4] *Department of Physics, Imperial College London, London SW7 2AZ, UK*
[5] *now at: Institute of Electronic Structure and Laser, Foundation for Research and Technology-Hellas, PO Box 1527, 71110 Heraklion, Greece*

(Dated: May 25, 2016)

We demonstrate quantum logic using narrow linewidth photons that are produced with an a-priory non-probabilistic scheme from a single ^{87}Rb atom strongly coupled to a high-finesse cavity. We use a controlled-NOT gate integrated into a photonic chip to entangle these photons, and we observe non-classical correlations between photon detection events separated by periods exceeding the travel time across the chip by three orders of magnitude. This enables quantum technology that will use the properties of both narrowband single photon sources and integrated quantum photonics.

Since the proposal of linear optical quantum computing (LOQC) [1] and hybrid quantum networking [2], achievements in both areas have been impressive. On the one hand, LOQC is harnessing increased control of single photons to enable new applications of photonic quantum technologies [3] and phenomena [4]. On the other hand, quantum interfacing of stationary with flying quantum bits (qubits) in the form of atoms and photons is now well under control in strong cavity coupling [5]. Here, we successfully combine these hitherto separate fields into a scheme which uses non-probabilistic atom-photon interfacing to deliver photons on demand. First, atomic states in strong cavity coupling are mapped to photons of narrow linewidth with a system that controls the temporal coherence profile [6, 7]. Second, we use an on-chip photonic network [8] to demonstrate quantum-controlled not (CNOT) and entangling operations acting on these photons. The overall similarity of our measurements with the expected outcome exceeds 90%, which shows that narrowband photons from atom-cavity systems used with integrated quantum photonics are promising for quantum information processing tasks. including photonic quantum computing [9], narrow linewidth quantum enhanced sensing [10] and atomic memories [11].

New applications of single photons will continue to emerge from increased control of both their emission and their processing with photonic components. Today, intrinsically probabilistic photon sources, such as spontaneous parametric down conversion, are widely used for proof-of-principle photonic quantum technologies. This is because of control over properties such as entanglement [12] and spectrum [10], and increasingly because of the demonstrated compatibility with integrated photonics [13]. But probabilistic sources can only generate high numbers of photons with an overhead of fast switching and optical delays [14]. Deterministic photon emitters circumvent this overhead whilst providing valuable capabilities such as mediating entangling operations and acting as quantum memories. Here we demonstrate that it is also possible to operate integrated quantum logic with ultra-narrowband photons emitted on-demand from single ^{87}Rb atoms.

Integrated optics is a viable approach to control photons with increasingly complex, miniature, and programmable quantum circuits [8, 13, 15], with capabilities significantly enlarged when used with reliable single-photon emitters. For instance, photons from single quantum dots have been used to measure the logical truth table of an on-chip controlled-NOT gate (CNOT) [16] and entangled using a bulk-optical CNOT [17], and photons emitted from diamond colour centres have been manipulated with an on-chip interferometer [18]. These emitters can be regarded as artificial atomic systems. In contrast to these, narrowband indistinguishable photons can be obtained on-demand from real atoms in strong coupling to high-finesse cavities [5, 19]. These systems emit mutually coherent photons [20], they have been used to generate photon-atom entanglement [21] and distant atom-atom entanglement [22], they can be used for quantum memories [23] and they can be used to individually tailor the phase and coherence envelope of each emitted single photon [6, 7]. We seek the benefits of both integrated quantum photonic circuits and atom-cavity photon sources.

Our demonstration operates integrated photonic quantum logic with single photons, emitted from ^{87}Rb atoms coupled to a high-finesse optical cavity [6, 24]. We encode qubits on each single photon, that occupies one of two optical waveguides to demonstrate two-qubit logic using a probabilistic CNOT gate [25, 26] integrated within a silica-on-silicon chip [8]. We verify that for successful gate operation, the two qubits become entangled. The photons have ultra-long coherence length which gives rise

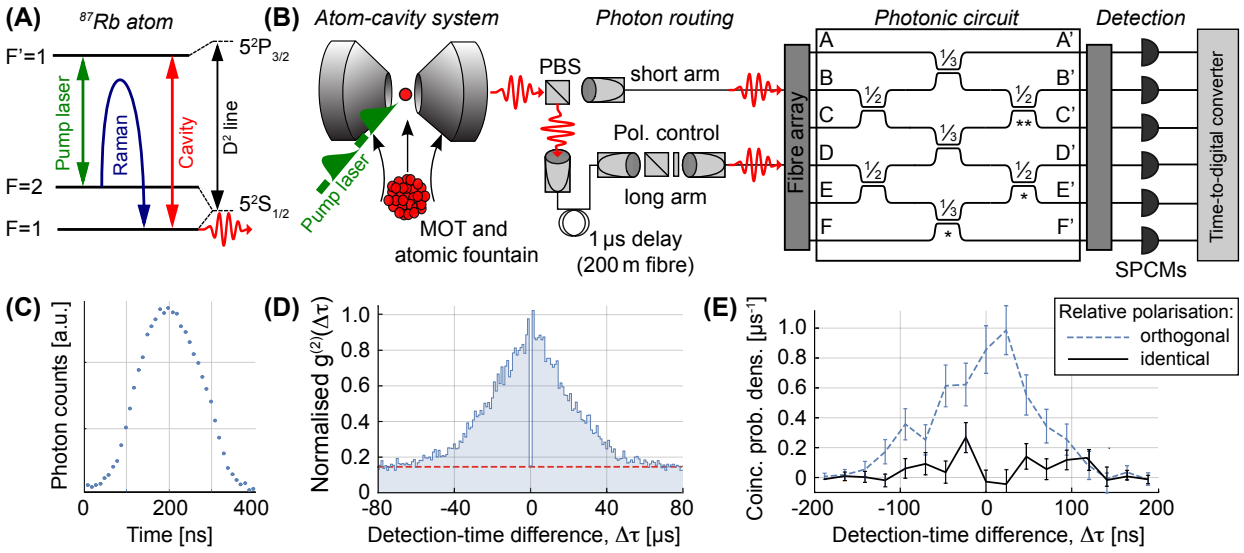

FIG. 1: Hybrid atom-cavity and photonic chip system: Vacuum-stimulated Raman transitions (A) between hyperfine ground states in ^{87}Rb control the production of single photons. An atomic fountain injects the atoms into a high-finesse optical cavity (B). Photons emitted from the cavity are delayed to simultaneously enter a photonic circuit, with single-photon counting modules (SPCMs) registering the photons at all outputs with a time-to-digital converter. The spatio-temporal envelope of the photons (C) is nearly symmetric on a 400 ns long finite support. (D) The second-order correlation $g^{(2)}(\Delta\tau)$, with temporal envelope restricted due to the finite atom-cavity 60 μs interaction time. The dashed line indicates the detector dark-count contribution to $g^{(2)}(\Delta\tau)$. (E) The time-resolved HOM interference pattern of two photons arriving at directional coupler "**" is shown by plotting the time-resolved probability density for detecting a coinciding photon in C' conditioned on a detection in B' (Coinc. prob. dens.), as a function of the time difference between detections. From this we obtain a visibility of 85(±5)%. We characterise the reflectivity of the directional couplers by guiding 780nm CW laser light through the chip and measuring relative output intensity, assuming uniform waveguide losses. We found the reflectivity of directional coupler "**" to be 53.4%, which limits the maximum visibility of HOM interference to be 99.1%.

to non-classically correlated detection events that are up to three orders of magnitude further apart than the time needed for light to travel across the chip. This agrees with previous measurements of time-resolved Hong-Ou-Mandel interference of long photons [20], from which we conclude that we entangle two ultra-narrowband qubits that can be used for quantum information protocols [9].

The experimental arrangement is illustrated in Fig. 1. Single photons of 60 m (200 ns) coherence length (corresponding to a bandwidth of 1.6 MHz) and a wavelength 780.2 nm are derived from a strongly coupled atom-cavity system. This is accomplished with a coherently controlled vacuum-stimulated Raman transition in ^{87}Rb with a repetition rate of 1 MHz and an efficiency $> 60\%$ [5, 6, 19, 24]. The source operates intermittently for periods of up to 60 μs due to the stochastic delivery of atoms to the cavity with an atomic fountain. To obtain pairs of photons, a polarising beam splitter (PBS) directs the unpolarised photon stream into a short or a long path—with a splitting ratio of $50\pm0.03\%$—chosen to delay one of the photons by the 1 μs period of the photon-generation sequence. Free space polarisation optics then control the polarisation of the photons input to the chip. Due to this random organisation of photons into two paths and insertion loss from collecting optical fibre, two consecutively emitted photons are simultaneously available with a typical likelihood of $\sim$ 12%. The rate of detected photon pairs is reduced further by photon loss across the chip and detector efficiencies (with figures of merit discussed below) but we note that the total loss throughout the reported setup is sufficiently low to enable photon pair data collection using post-selection.

The photonic circuit, shown in Fig. 1(B), is a network of single-mode waveguide directional couplers designed to operate in the near-infrared (NIR) and fabricated lithographically using germanium and boron doped silica on a silicon substrate [8]. The buried square 3.5 μm $\times$3.5 μm waveguides of refractive index contrast $\Delta n = 0.5\%$ support only the fundamental mode at 780 nm. For photons from spontaneous parametric down conversion with a coherence length in the 100 μm range, the quantum processes for single- and two-qubit logic using exactly this architecture has been characterised [15]. The input and output facets of the chip are glued with an optical adhesive to polarisation maintaining fibre arrays to simplify coupling. The average loss across the chip from input to output fibre is 3.3 dB. Photons emerging at the output ports get detected by commercial silicon avalanche photodiodes with a typical quantum efficiency of 70% and a time resolution of 300 ps which is three orders of magni-

tude smaller than the photonic coherence length or repetition rate of the source. Every event is recorded and all photon-photon coincidence statistics are extracted from this data.

The photonic chip is used in a Hanbury-Brown-Twiss configuration [27] at directional couplers "$*$" to characterise the photon-emission statistics of the atom-cavity system. Photons are sent along a single path into input F and from the pair correlations between outputs D', E', and F' we measure the second-order correlation function $g^{(2)}(\Delta\tau)$ shown in Fig. 1(D). The source operates intermittently [28], so that the maximum of this trace corresponds to the uncorrelated case with $g^{(2)}_{\max} = 1$. The finite atom-cavity interaction leads to the signal tailing off to both ends. At time delay $\Delta\tau = 0$, $g^{(2)}(0) = 0.15$ indicates the reduction in probability of detecting two events during a single trigger pulse. These residual correlations can be fully attributed to detector dark counts; the shot noise of which imposes an upper limit of $g^{(2)}(0) < 0.02$ to the photon stream at the one-sigma confidence level.

The mutual coherence and indistinguishability of photons is verified by time-resolved Hong-Ou-Mandel (HOM) interference of two photons [20, 29, 30]. Photons from the long and short arms are directed into ports A and D. Their interference at the directional coupler "$**$" determines the photon-photon coincidences between detectors monitoring outputs B' and C', shown in Fig. 1(E) as a function of the detection-time difference. Upon transitioning from non-interfering photons of orthogonal polarisation to interfering photons of identical polarisation, the likelihood for coincidences drops by $85(\pm5)\%$. This large visibility of the HOM effect quantifies the degree to which our hybrid setup prepares and preserves indistinguishability of all properties of the photons.

We use the photonic chip as a linear optical CNOT gate [8] as shown in Fig. 2(A) [37]. This gate flips the state of a target qubit conditional on the state of a control qubit. The qubits are realised in the photon pairs emitted from the cavity, with one photon guided into C_0 or C_1 and the other into T_0 or T_1. The gate's mechanism is based on two core principles of linear optics [9]: single photon interference in the interferometer acting on T_0 and T_1, and HOM interference at a nominally $\eta = 1/3$ reflectivity directional coupler. Operation of the gate is post-selected upon detection of one photon in C_0 or C_1 and another photon in T_0 or T_1, which occurs with probability $P_s = 1/9$, as defined by the reflectivity of the nominally $\eta = 1/3$ couplers [25, 26]. We estimate from characterisation that these couplers have reflectivity of $\eta = 0.35 \pm 0.02$, from which we estimate that the minimum success rate of the gate over all input states is $P_s = 0.09 \pm 0.02$. The logical truth table shown in Fig. 2(B) is derived from the ensemble of control-target correlated detections measured across the coherence envelope of the photons. The data is corrected for background counts and normalised using maximum likelihood estimation (MLE) [31]. Our results show a similarity of $S = 94(\pm1)\%$ with the ideal CNOT truth table, which increases to $S = 97(\pm1)\%$ if we account for non-ideal directional coupler reflectivities and phase shifts, that we characterise using a 780 nm CW laser. Without subtracting background, the measured truth table has a similarity of $85 \pm 1.5\%$ with the ideal truth table [38]. We use $S = \sum \sqrt{p_i q_i} / \sqrt{\sum p_i \sum q_i}$, where p_i and q_i are elements of the measured and expected truth tables. This measure is also used to partly characterise previous demonstrations of integrated photonic quantum logic (e.g. [8]). For reference, if the chip was operating as a perfect identity channel then it would yield $S = 50\%$, and in the case of no quantum interference a perfect optical chip would give $S = 79\%$. Due to the long coherence time of the photons, we also observe correlated detection events that are notably separated in time. From these, we determine the similarity with the expected truth table as a function of the detection-time difference, see Fig. 2(C). With the coherence length of the photons surpassing the gate dimensions (10 mm, or 33 ps) by three orders of magnitude, the gate operates as expected for detections up to 100 ns apart. Beyond that, the event rate is too small compared to noise which then dominates the data.

We emphasise that by itself similarity of a lone logical truth table does not characterise ability to perform coherent operation on superposition of qubit states and should not be mistaken for quantum fidelity. Nonetheless a defining feature of two-qubit logic is the ability to generate entanglement from separable input states. Bounding the quantum state fidelity $F_{|\psi^+\rangle}$ of our output state with an ideal entangled state $|\psi^+\rangle$ enables comparison to other experiments that have generated entanglement, including with similar linear optics schemes (e.g. [15, 17]). The combination of the first Hadamard and the CNOT in Fig. 3 generates the maximally entangled $|\psi^+\rangle = \frac{1}{\sqrt{2}}(|01\rangle_{CT} + |10\rangle_{CT})$ Bell state. We verify the presence of entanglement by measuring correlations between Pauli operators along both the z- and x-axes [32, 33]. A Sagnac loop is connected to reuse part of the chip backwards as shown in Fig. 3(C) and (D), to allow measurement of the expectation values of the observables $Z \otimes Z$ and $X \otimes X$ [39]. We reconstruct the probability distributions for these two values using MLE, with the data normalised to the logical two-bit basis, shown in Fig. 3(A) and (B) respectively. The correlations show similarities of $97(\pm3)\%$ and $94(\pm2)\%$ with the ideal distributions. Using these measurements we can lower bound the quantum state fidelity to the $|\psi^+\rangle$ state by $F_{|\psi^+\rangle} \geq \frac{1}{2}(-\langle Z \otimes Z\rangle + \langle X \otimes X\rangle)$ [33], where any state with $F_{|\psi^+\rangle} > 0.5$ is entangled [34]. Our data yields $F_{|\psi^+\rangle} \geq 0.82(\pm0.10)$ [40]. Much like the similarity shown in Fig. 2(C), the degree of entanglement is largely insensitive to the detection-time difference. We are able to observe non-classical correlations between pairs of photons that are projected onto states that could not have

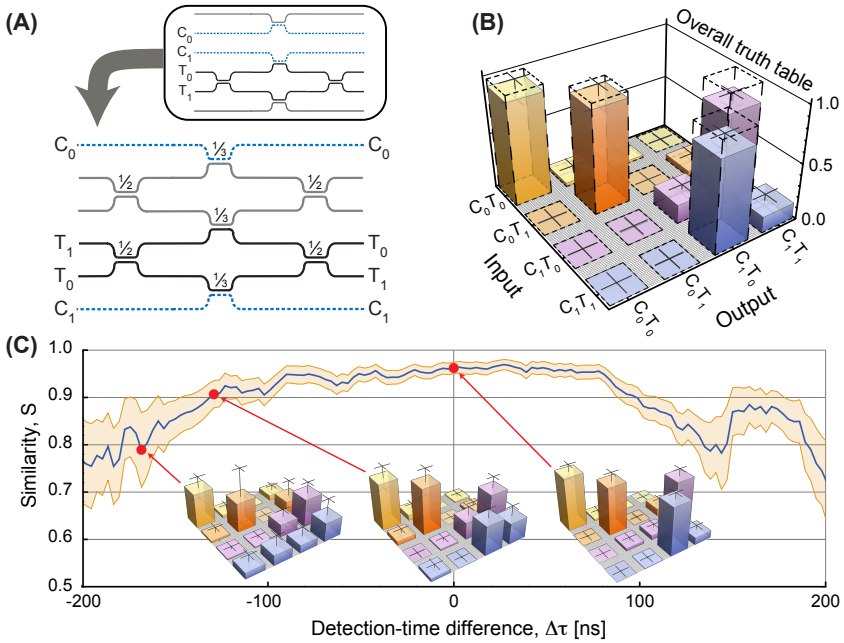

FIG. 2: Linear optical CNOT gate operating on cavity photons: (A) shows the mapping of dual-rail encoded qubits to the channels of the chip we use. The overall truth table in the coincidence basis (B) is derived from 1110 pairs of control–target correlations detected up to ±200 ns apart and measured within 20 hours. Ideal CNOT operation is presented by dotted bars. (C) Similarity of the truth table with the ideal CNOT as a function of the separation between detections, $\Delta\tau$. Events are considered within $\Delta\tau \pm 30$ ns. For detections up to 100 ns apart, the similarity exceeds 90%. Beyond that, it drops due to noise dominating the signal. This is evident by correlations arising for which there is no path routing the input photons to those output channels.

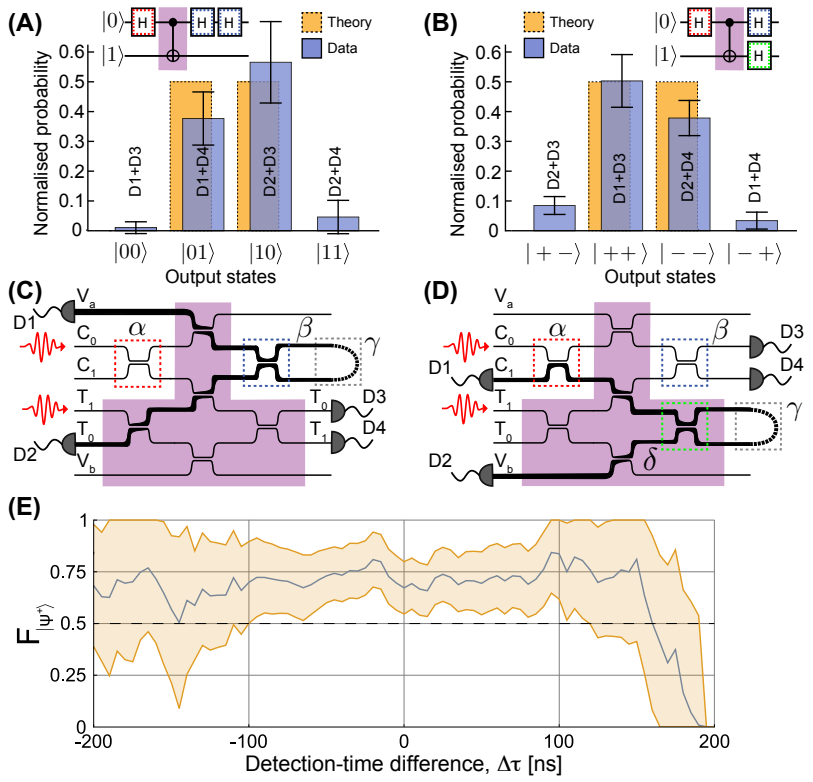

FIG. 3: Non-classical qubit correlations. The circuits in (A, B) illustrate the Hadamard and CNOT gates used to measure expectation values of $Z \otimes Z$ and $X \otimes X$. The top (bottom) rail corresponds to the control (target) qubit. (A,B) The measured and ideal measurement outcomes for these two configurations. Error bars are computed assuming Poisson distributed noise on the total detection events, including from background noise. We then subtract measured background noise, leading to error bars that drop below zero in (A). (C,D) Experimental implementations of configurations (A,B). The directional coupler α rotates the control qubit into the X-basis, which the CNOT (shaded region) entangles with the target qubit into the state $|\psi^+\rangle$. (C) The fibre Sagnac loop (γ) redirects the control back through through the chip along the bold path (through β again), to rotate the control qubit back into the Z-basis. (D) The Sagnac loop now leaves the control-qubit in the X-basis and rotates the target qubit that now follows the bold path (through δ again) into the X-basis. Detections at detectors D1, D2, D3, D4 correspond to measurements of the states $|0\rangle_C$, $|1\rangle_C$, $|0\rangle_T$, $|1\rangle_T$ in (C) and $|+\rangle_T$, $|-\rangle_T$, $|+\rangle_C$, $|-\rangle_C$ in (D). (E) Variation of fidelity bound for $|\psi^+\rangle$ when considering only a subset of the detections, separated by $\Delta\tau \pm 50$ ns.

occupied the optical chip simultaneously. Seemingly the trace in Fig. 3(E) remains below the computed bound of 0.82. We can attribute this to statistical noise affecting the subsets of data evaluated for each point of the trace in an unfavourable way. Even in the centre of the trace where the signal to random noise of the experiment is highest, the statistical noise due to the paucity of events still suppresses the bound of $F_{|\psi^+\rangle}$ computed with smaller datasets. Qualitatively Fig. 3(E) shows that quantum interference is unaffected by photon localisation in time or

space that one could otherwise associate with the two separate photon detections.

We have shown the reliable operation of two-qubit linear optical quantum gates and generated photon-photon entanglement [9] applied to photons emitted from a single atom strongly coupled to a cavity. Immediately, this new platform can be used for other two-photon experiments that exploit simultaneously the capabilities of integrated quantum photonics and atom-cavity systems. In the current experiment the photons were passively routed—active switching of the photons using an off the shelf EOM would allow for deterministic routing, thus increasing the number of pairs entering the chip by a factor of four. Improving overall system efficiency and deterministic loading of atoms into cavities will increase the capability of this system to larger photon-number. Our photon rates reported here of 1110 pairs in twenty hours includes the full time span during which our intermittently operating source is inactive. In fact, 1110 pairs are actually detected within an active time span of an atom occupying the cavity of 21 seconds. This is the figure that should be considered for any estimate regarding the feasibility of scaling by trapping of atoms in cavities [35]. We note that while the potential detrimental effects of trapping atoms has on the indistinguishability of emitted photons is yet to be studied in full, compatibility of such systems are being reported—narrowband photons emitted from one atom-cavity system have been absorbed with high fidelity by another [22].

Acknowledgements: We thank A. Politi for his efforts on the design of the photonic chip. This work was supported by EPSRC, ERC, BBOI, PHORBITECH, QUANTIP, US Army Research Office (ARO) Grant No. W911NF-14-1-0133, U.S. Air Force Office of Scientific Research (AFOSR) and the Centre for Nanoscience and Quantum Information (NSQI). G.D.M. acknowledges the FP7 Marie Curie International Incoming Fellowship scheme. J.L.O'B. acknowledges a Royal Society Wolfson Merit Award and a Royal Academy of Engineering Chair in Emerging Technologies. A.K. acknowledges EPSRC support through the quantum technologies programme (NQIT hub) and by the German Research Foundation (DFG, RU 635). J.C.F.M. was supported by a Leverhulme Trust Early Career Fellowship. The authors are grateful to *ένα γρου ρακί* for stimulating discussion and to D. Stuart and T. Barrett for extensive proof-reading and their most helpful comments.

[1] E. Knill, R. Laflamme, and G. J. Milburn, Nature **409**, 46 (2001).
[2] J. I. Cirac, P. Zoller, H. J. Kimble, and H. Mabuchi, Phys. Rev. Lett. **78**, 3221 (1997).
[3] J. L. O'Brien, A. Furusawa, and J. Vuckovic, Nature Photon **3**, 687 (2009).
[4] P. Shadbolt, J. C. F. Matthews, A. Laing, and J. L. O'Brien, Nat Phys **10**, 278 (2014).
[5] A. Kuhn, in *Engineering the Atom-Photon Interaction*, edited by A. Predojevic and W. Mitchell (Springer, 2015), chap. 1, pp. 3–35.
[6] P. B. R. Nisbet-Jones, J. Dilley, D. Ljunggren, and A. Kuhn, N. J. Phys. **13**, 103036 (2011).
[7] J. Dilley, P. Nisbet-Jones, B. W. Shore, and A. Kuhn, Phys. Rev. A **85**, 023834 (2012).
[8] A. Politi, M. J. Cryan, J. G. Rarity, S. Yu, and J. L. O'Brien, Science **320**, 646 (2008).
[9] P. Kok, W. J. Munro, K. Nemoto, T. C. Ralph, J. P. Dowling, and G. J. Milburn, Rev. Mod. Phys. **79**, 135 (2007).
[10] F. Wolfgramm, C. Vitelli, F. A. Beduini, N. Godbout, and M. W. Mitchell, Nature Photon. **7**, 28 (2013).
[11] H. P. Specht, C. Nolleke, A. Reiserer, M. Uphoff, E. Figueroa, S. Ritter, and G. Rempe, Nature **473**, 190 (2011).
[12] P. G. Kwiat, K. Mattle, H. Weinfurter, A. Zeilinger, A. V. Sergienko, and Y. H. Shih, Phys. Rev. Lett. **75**, 4337 (1995).
[13] J. W. Silverstone, D. Bonneau, K. Ohira, N. Suzuki, H. Yoshida, N. Iizuka, M. Ezaki, C. M. Natarajan, M. G. Tanner, R. H. Hadfield, et al., Nat. Photon. **8**, 104 (2014).
[14] A. L. Midgall, D. Branning, and S. Castelletto, Phys. Rev. A **66**, 053805 (2002).
[15] P. J. Shadbolt, M. R. Verde, A. Peruzzo, A. Politi, A. Laing, M. Lobino, J. C. F. Matthews, M. G. Thompson, and J. L. O'Brien, Nature Photonics **6**, 45 (2012).
[16] M. A. Pooley, D. J. P. Ellis, R. B. Patel, A. J. Bennett, K. H. A. Chan, I. Farrer, D. A. Ritchie, and A. J. Shields, Appl. Phys. Lett. **100**, 211103 (2012).
[17] O. Gazzano, M. P. Almeida, A. K. Nowak, S. L. Portalupi, A. Lemaitre, I. Sagnes, A. G. White, and P. Senellart, Phys. Rev. Lett. **110**, 250501 (2013).
[18] J. E. Kennard, J. P. Hadden, L. Marseglia, I. Aharonovich, S. Castelletto, B. R. Patton, A. Politi, J. C. F. Matthews, A. G. Sinclair, B. C. Gibson, et al., Phys. Rev. Lett. **111**, 213603 (2013).
[19] A. Kuhn, M. Hennrich, and G. Rempe, Phys. Rev. Lett. **89**, 067901 (2002).
[20] T. Legero, T. Wilk, M. Hennrich, G. Rempe, and A. Kuhn, Phys. Rev. Lett. **93**, 070503 (2004).
[21] T. Wilk, S. C. Webster, A. Kuhn, and G. Rempe, Science **317**, 488 (2007).
[22] S. Ritter, C. Nölleke, C. Hahn, A. Reiserer, A. Neuzner, M. Uphoff, M. Mücke, E. Figueroa, J. Bochmann, and G. Rempe, Nature **484**, 195 (2012).
[23] M. Khudaverdyan, W. Alt, I. Dotsenko, T. Kampschulte, K. Lenhard, A. Rauschenbeutel, S. Reick, K. Schorner, A. Widera, and D. Meschede, New J. Phys. **19**, 073023 (2008).
[24] P. B. R. Nisbet-Jones, J. Dilley, A. Holleczek, O. Barter, and A. Kuhn, N. J. Phys. **15**, 053007 (2013).
[25] T. C. Ralph, N. K. Langford, T. B. Bell, and A. G. White, Phys. Rev. A **65**, 062324 (2002).
[26] H. F. Hofmann and S. Takeuchi, Phys. Rev. A **66**, 024308 (2002).
[27] R. Hanbury Brown and R. Twiss, Nature **178**, 1046 (1956).
[28] M. Hennrich, T. Legero, A. Kuhn, and G. Rempe, New Journal of Physics **6**, 86 (2004).
[29] C. K. Hong, Z. Y. Ou, and L. Mandel, Phys. Rev. Lett. **59**, 2044 (1987).
[30] T. Legero, T. Wilk, A. Kuhn, and G. Rempe, Adv. At. Mol. Opt. Phys. **53**, 253 (2006).
[31] J. W. Harris and H. Stocker, *Handbook of Mathematics and Computational Science* (Springer, NY, 1998), chap. 21.10.4: Maximum Likelihood Method, p. 824.
[32] K. M. R. Audenaert and M. B. Plenio, New J. Phys. **8**,

266 (2006).
[33] H. Wunderlich and M. B. Plenio, J. Mod. Opt. **56**, 2100 (2009).
[34] B. M. Terhal and P. Horodecki, Phys. Rev. A **61**, 040301 (2000).
[35] M. Hijlkema, B. Weber, H. P. Specht, S. C. Webster, A. Kuhn, and G. Rempe, Nature Physics **3**, 253 (2007).
[36] F. Marsili, V. B. Verma, J. A. Stern, S. Harrington, A. E. Lita, T. Gerrits, I. Vayshenker, B. Baek, M. D. Shaw, R. P. Mirin, et al., Nat Photon **7**, 210 (2013).
[37] In contrast to the standard schematic [25, 26], here the vacuum modes get mixed on the chip. This does not affect the overall operation of the circuit as a CNOT gate.
[38] Note that un-corrected raw data can be improved with detectors with reduced dark counts and high efficiency, such as superconducting nanowire single photon detectors [36]
[39] Note that the matrix representation of a directional coupler is a symmetrical and complex version of the Hadamard operation. Here we account for this by relabelling qubit states [8]. The relabelling does not alter observing the amount of entanglement observed by bounding $F_{|\psi^+\rangle}$.
[40] The non-ideal directional coupler reflectivities and phases in the interferometers preclude us from measuring $F_{|\psi^+\rangle} \geq 0.87$.